From caged compounds with isolated U atoms to frustrated magnets with 2- or 3-atom clusters: a review of Al-rich uranium aluminides with transition metals

Mathieu Pasturel, Adam P. Pikul

From caged compounds with isolated U atoms to frustrated magnets with 2- or 3-atom clusters: a review of Al-rich uranium aluminides with transition metals

Mathieu Pasturel[1] **& Adam Pikul**[2,3]

[1] Univ Rennes, CNRS, Institut des Sciences Chimiques de Rennes - UMR6226, 35042 Rennes, France

[2] Institute of Low Temperature and Structure Research, Polish Academy of sciences, 50-422 Wroclaw, Poland

[2] Centre for Advanced Materials and Smart Structures, Polish Academy of sciences, 50-422 Wroclaw, Poland

E-mail: mathieu.pasturel@univ-rennes1.fr; a.pikul@intibs.pl

2 March 2023

Abstract. Crystal structures and physical properties of four families of Al-rich ternary uranium compounds with transition metals (TE) are reviewed, namely UTE_2Al_{20}, UTE_2Al_{10}, $U_6TE_4Al_{43}$, and $U_3TE_4Al_{12}$. The compounds can be described as consisting of 1 (isolated), 2 (dumbbells) or 3 (triangles) uranium atom clusters, surrounded (1-2-20, 1-2-10 and 6-4-43) or not (3-4-12) by large cages, which strongly influence their magnetic and related properties. Indeed, the ground states of the described systems evolve from Curie-like paramagnetism in the case of the phases with well-isolated, single U-atoms, to complex magnetic order or frustrated magnetism in the case of the systems with uranium triangles forming a breathing kagome lattice. We argue that the four families of uranium aluminides described in this review provide a unique opportunity to study magnetic interactions between U magnetic moments while gradually increasing the number of their nearest magnetic neighbors, and may also be helpful in understanding the fundamental origin of magnetic freezing phenomena.

Submitted to: *Rep. Prog. Phys.*

Introduction

Thanks to their isotropic irradiation behaviour, relatively high uranium density, high thermal conductivity, proper fission gases accommodation and easy synthesis, binary uranium aluminides have been used for decades as nuclear fuels for research and test reactors (RTRs) (Nazaré et al. 1975, Dienst et al. 1977), as well as fissile material for irradiation targets for the production of medical radioisotopes (Ryu

et al. 2013, Raposio et al. 2019, Durazzo et al. 2021). The binary U-Al phase diagram is quite simple and contains only three binary phases: the cubic phase UAl_2 (space group $Fd\bar{3}m$, structure type $MgCu_2$, $\rho \approx 8.1\,\mathrm{g\,cm^{-3}}$), the cubic phase UAl_3 ($Pm\bar{3}m$, Cu_3Au, $\rho \approx 6.8\,\mathrm{g\,cm^{-3}}$), and the orthorhombic phase UAl_4 ($Imma$, own structure type, $\rho \approx 6.1\,\mathrm{g\,cm^{-3}}$). Their uranium densities ρ_U are rather moderate (6.6 $g_U\,cm^{-3}$, 5.0 $g_U\,cm^{-3}$ and 4.2 $g_U\,cm^{-3}$, respectively), so they imply the use of highly enriched uranium in RTRs and irradiation targets to achieve higher performances (the desired ^{235}U content is above 90%, while natural U contains only about 0.7% of ^{235}U). However, since international non-proliferation treaties limit civilian uranium enrichment of a maximum of 20%, the use of the binary uranium aluminides mentioned above is not an optimal choice. Therefore, higher U-density nuclear fuels are needed to compensate for the lower enrichment. Among them, transition metal-stabilised high-temperature cubic γ-allotropes of uranium are highly promising. For instance, the addition of approximately 7 – 10 wt% of molybdenum to uranium has been intensively studied as a fuel for RTRs due to the high chemical stability of the γ-U(Mo) phase, its stability under irradiation and the increased density of uranium ($\rho_U \approx$ 16-17 $g_U\,cm^{-3}$) (Snelgrove et al. 1997, Leenaers et al. 2020a). Other materials under consideration include U_3Si_2 ($\rho_U \approx 11.3\,g_U\,cm^{-3}$) (Leenaers et al. 2020b), UN ($\rho_U \approx 13.5\,g_U\,cm^{-3}$) (Durand & Laudamy 1994, Wallenius 2020), UC ($\rho_U \approx 13.0\,g_U\,cm^{-3}$) (Clement Ravi Chandar et al. 2020) and UB_2 ($\rho_U \approx 11.7\,g_U\,cm^{-3}$) (Turner et al. 2020) among others.

Further technological development of the metallic fuels requires excellent knowledge of their behaviour during fabrication and operation, including their reactivity with Al matrix (note that the RTRs fuels and irradiation plates are mostly a mixture of the U-bearing powder with Al powder for mechanical resistance and heat dissipation), with cladding materials (usually made of Al, Zr, Ti or Ni) and with fission products. In many cases, this reactivity can be predicted using binary, ternary and quaternary (or more) phase diagrams. Several isothermal sections of such diagrams have been reported in recent decades with the following objectives: (i) U-Al-Si for the reactivity between U_3Si_2 and Al matrix (Rabin et al. 2015), (ii) U-TE-Al with TE = Mo (Noël et al. 2009) and Nb (Moussa et al. 2017) for the reactivity of γ-U(TE) fuels with Al matrix, (iii) U-TE-Al with TE = Ti (Moussa, Pasturel, Stepnik & Tougait 2015), Zr (Moussa, Désévédavy, Noël, Pasturel, Gouttefangeas, Dubois, Stepnik & Tougait 2015) and Fe (Gonçalves & Noël 2005) for the reactivity of UAl_x fuels with cladding, and many others.

In addition to obtaining technologically relevant information, the study of the U-TE-Al phase diagrams (where TE is usually a transition element and sometimes a p-block element) confirms or reveals the existence of binary and ternary aluminides of potential importance from a fundamental physics point of view. This has to do with the fact that the $5f$ orbitals of actinides in general (and uranium in particular) are an intermediate case in terms of radial extension between the outer nd orbitals of the transition elements and the inner $4f$ orbitals of the rare earth elements. As such, they are sensitive to both the crystal field effect (energy dominant for $3d$ elements) and spin-orbit coupling (leading for the $4f$ elements). In many cases, this implies a strong dependence

of the physical properties on the distance between U atoms ($d_{\mathrm{U-U}}$) or between U atoms and ligands. In particular, as shown empirically by Hill in 1970, the distance between two uranium atoms of about 3.4 – 3.6 Å favors the occurrence of magnetic ordering (Hill 1970). Shorter U–U distances lead to strong hybridization of the $5f$ orbitals with the conduction electrons, which results in delocalization of the $5f$ electrons and – in most cases – weak Pauli paramagnetism of the compound (see *e.g.* ht-UFeAl with $d_{\mathrm{U-U}} \approx 3.0$ Å (Troć et al. 1993)). On the other hand, larger $d_{\mathrm{U-U}}$ values lead often to hard ferromagnetism with elevated Curie temperature (see *e.g.* $U_3Al_2(Si,Ge)_3$ with $d_{U-U} \approx 4.0$ Å (Weitzer et al. 1994) or UPtAl with $d_{U-U} \approx 3.6$ Å (Andreev et al. 1999)).

Furthermore, examination of the aluminum-rich corners of the ternary U-TE-Al phase diagrams also revealed quite complex and interesting crystallochemistry of the ternary compounds. In particular, the U atoms can form various sublattices in those systems: from a sublattice of isolated U atoms in large cages made of ligands (as in the compounds UTE_2Al_{20} with TE = Ti, V, Nb, Ta, Cr, Mo, W, Mn, or in UTE_2Al_{10} with TE = Fe, Ru, and Os), to a three-dimensional sublattice of isolated U dumbbells (as in $U_6TE_4Al_{43}$ with TE = V, Nb, Ta, Cr, Mo, and W) or U triangles (as in $U_3TE_4Al_{12}$ with TE = Fe, Ru, and Co). Interestingly, the physical properties of the compounds in the latter two families were found to be dominated by frustrated magnetism, caused either by the interplay between the short- and long-range interactions, or the inability of magnetic moments to order themselves in a pure antiferromagnetic state in a triangular lattice. Because of their chemical similarity, the study of those systems can therefore be very helpful in better understanding the physics of systems with isolated groups of 1, 2 or 3 uranium atoms, as well as the physics of frustrated systems.

This short review therefore aims to present the state of the art of the most relevant results reported for the compounds UTE_2Al_{20} and UTE_2Al_{10} (Sec. 1), $U_6TE_4Al_{43}$ (Sec. 2), and $U_3TE_4Al_{12}$ (Sec. 3). Their properties are compared and discussed in Sec. 4, not only to provide a general overview of these compounds, but also to try to relate the chemical and crystallographic characteristics to their magnetic properties.

1. Cage compounds UTE_2Al_{20} and UTE_2Al_{10}

1.1. Crystal structure

The crystal chemistry of the Al-rich, ternary U-TE-Al phases strongly depends on the position of TE in the periodic table of elements. In particular, for the low-number columns (*i.e.* for TE = Ti, V, Nb, Ta, Cr, Mo, W, and Mn), the formation of cubic phases UTE_2Al_{20} with the structure-type $CeCr_2Al_{20}$ was reported, while for the 8^{th} column (for TE = Fe, Ru, and Os), the existence of orthorhombic compounds UTE_2Al_{10} adopting the structure type $YbFe_2Al_{10}$ was discovered.

For the transition elements from the high-number column, much fewer information is available in the literature. The isothermal section of the ternary phase diagram U-Co-Al at 900°C, reported by Noël *et al* (Noël et al. 2005), revealed the formation

of the monoclinic compound $U_2Co_6Al_{19}$ as the most aluminum-rich phase. For the system U-Cu-Al, Verbovytskyy and Gonçalves reported the existence of the tetragonal compound UCu_4Al_8 as the Al-richest phase among those found at 600°C (Verbovytsky Yu & Gonçalves 2013). However, due to their distinctly different crystal structure and rather preliminary character of the published information on their magnetic and related properties (Tougait et al. 2003, Troć et al. 2004, Geibel et al. 1990), they will not be discussed further in this review.

The crystal structures of UTE_2Al_{20} and UTE_2Al_{10} are shown in figure 1. The former phases all crystallize in a cubic structure of the $CeCr_2Al_{20}$ type with a space group $Fd\bar{3}m$ (no. 227) and a cell parameter between 14 and 15 Å (Niemann & Jeitschko 1995b, Okuda et al. 1989, Wang et al. 2010), while the latter systems adopt the orthorhombic $YbFe_2Al_{10}$-type structure with a space group $Cmcm$ (no. 63) and cell parameters a and c close to 9 Å, and b slightly larger than 10 Å (Meshi et al. 2002, Sugai et al. 2011, Troć et al. 2011). A common feature of these families of compounds is the caged nature of the uranium coordination sphere. In particular, in UTE_2Al_{20} the uranium atoms are surrounded by an almost regular Frank-Kasper polyhedron composed of 16 aluminum atoms with U-Al distances (above 3.1 Å) greater than the sum of metallic radii of these elements (*i.e.* $\Sigma = 2.99$ Å), while the Al-Al distances (from about 2.7 Å) are less than the corresponding sum of metallic radii ($\Sigma = 2.86$ Å). The importance of the Mo-Al and Al-Al bonds for the stability of the structure compared to the U-Al bond was confirmed by DFT calculations, *e.g.* in the case of UMo_2Al_{20} (Liu et al. 2017). In turn, UTE_2Al_{10}, the U atoms are surrounded by a more distorted cage of 16 Al atoms and 4 TE atoms. As in the previous family of compounds, the U-ligand distances are greater than 3.1 Å, while the Al-Al and Al-TE distances are less than the sum of their metallic radii.

As is well known, such cage features can lead to low thermal conductivity of, for example, thermoelectric materials due to the occurrence of the heavy element rattling phenomenon, which is responsible for strong phonon scattering (see (Ghosh et al. 2022) and references therein). Other interesting physical phenomena that have been observed in cage compounds include the superconductivity found in the phases $LaTE_4P_{12}$ (Meisner 1981), among others.

From a magnetism point of view, the distance between the uranium atoms in both the 1:2:20 and 1:2:10 series (above 6 and 5 Å, respectively) is significantly greater than the Hill criterion. Thus, little or no overlap of 5f orbitals is expected, and perhaps weak interactions between uranium magnetic moments and lack of magnetic ordering. Whether this hypothesis turned out to be true, we will show below, where we provide an overview of the physical properties of all the aluminides from the two families studied so far.

1.2. Physical properties of UTE_2Al_{20}

UTi_2Al_{20} Physical properties of UTi_2Al_{20} were first studied by Matsumoto *et al* (Matsumoto et al. 2013) using single crystals. DC magnetization measurements in a

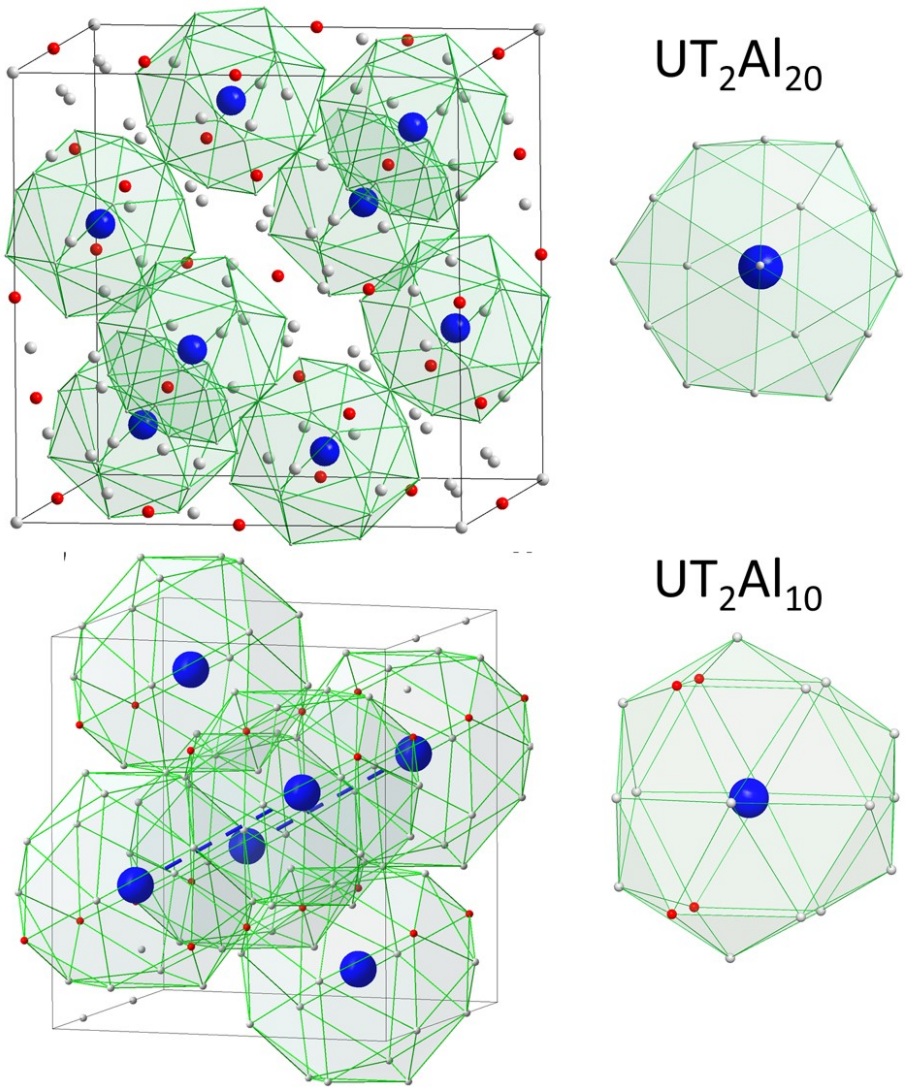

Figure 1. Crystal structures of UTE_2Al_{20} (top) and UTE_2Al_{10} (bottom) along with coordination polyhedra around U atoms in both types of structures. U atoms are shown as large blue spheres, TE-atoms are plotted as small red spheres, and Al is shown in grey. U-U distances of about 5 Å are shown as blue dashed lines, all the other ones being much larger than this value.

magnetic field parallel to the crystallographic direction [110] showed that the system is most likely a Pauli paramagnet with some Curie-like contribution from unspecified paramagnetic impurities. Comparison of the experimental data with the theoretical magnetic susceptibility curve calculated for free U^{4+} ions led the authors to conclude that the electron configuration of uranium in UTi_2Al_{20} is different than $5f^2$ and that the f-electrons in this system are itinerant in nature. Electrical resistivity of the compound measured along the direction [111] was found to be consistent with its paramagnetic properties (fig. 2). It shows no anomalies that could indicate any magnetic ordering, and below about 10 K it exhibits Fermi liquid-like behaviour $\rho(T) = \rho_0 + AT^2$ with the coefficient A of about $0.005\,\mu\Omega\,\mathrm{cm\,K^{-2}}$ (Matsumoto et al. 2013). Interestingly, one can

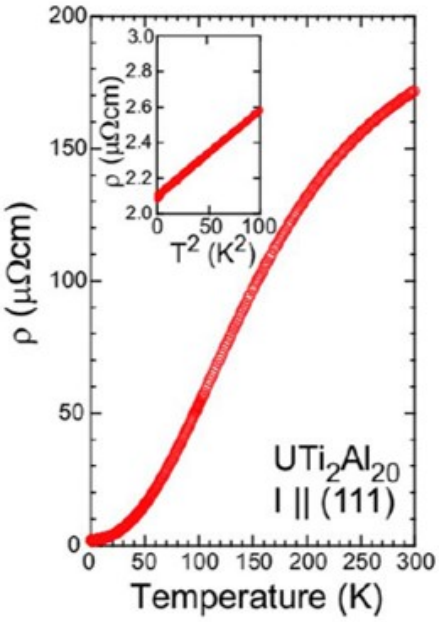

Figure 2. Temperature dependence of the electrical resistivity of UTi_2Al_{20}. Reproduced with permission from (Matsumoto et al. 2013).

also notice a broad hump on the $\rho(T)$ curve at elevated temperatures (roughly between 100 and 300 K), which is often observed in systems with spin fluctuations or (especially in intermetallic compounds with rare earth elements) in systems with the Kondo effect in the presence of crystal field.

UV_2Al_{20} The existence, crystal structure and basic physical properties of UV_2Al_{20} were first reported by Halevy *et al* for polycrystalline samples (Halevy et al. 2001). They found that the magnetic susceptibility of this cubic phase obeys the Curie-Weiss law with the effective magnetic moment $\mu_{\rm eff} = 2.3(3)\,\mu_{\rm B}/{\rm U}$, and that the compound does not order magnetically at least down to 1.7 K (no anomalies were observed in temperature variation of its magnetic susceptibility and electrical resistivity). High-pressure XRD experiments showed that there is no structural phase transition in UV_2Al_{20} at least up to 31.5 GPa. Paramagnetic ground state of the compound was confirmed by Wang *et al* (Wang et al. 2010).

Later, re-examination of the compound was carried out by Winiarski *et al* , also on polycrystalline samples (Winiarski et al. 2017). These independent studies revealed that the composition of the compound may be slightly sub-stoichiometric, namely close to $U_{0.8}V_2Al_{20}$. In addition, its paramagnetic ground state was confirmed, and the low-temperature electronic specific heat coefficient γ was estimated to be approximately $60\,{\rm mJ\,K^{-2}mol^{-1}}$.

Electronic structure of UV_2Al_{20} was calculated in the LDA approximation with the Perdew-Wang exchange-correlation potential using the fully-relativistic FPLO code by Swatek *et al* (Swatek et al. 2018). They showed that the 5f electrons of uranium are

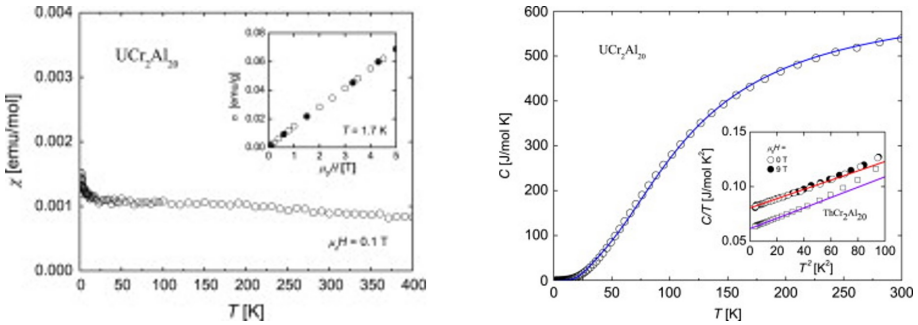

Figure 3. Temperature dependence of the magnetic susceptibility (left) and specific heat (right) of UCr_2Al_{20}. Reproduced with permission from (Swatek & Kaczorowski 2012).

strongly delocalized by coupling to their surroundings through hybridization between f orbitals with the d and p orbitals of neighbouring atoms, implying a significant contribution of U-5f states to the density of states near the Fermi level. According to the calculations, the $f-p$ hybridization is the most dominant process – its energy accounts for about 98% of the total hybridization energy. As expected, the direct overlap of f orbitals is very small, which is consistent with Hill limit mentioned earlier, but – due to the strong f–d and f–p hybridization – does not lead to any magnetic ordering.

UCr_2Al_{20} Physical properties of UCr_2Al_{20} were first reported by Okuda *et al* for a polycrystalline sample (Okuda et al. 1989). They suggested that this compound is ferromagnetically ordered below a surprisingly high temperature of 180 K with an extremely low saturated magnetic moment of the order of $4\times10^{-3}\,\mu_B$ per uranium atom.

Later studies (Swatek & Kaczorowski 2012) performed on high-quality single-crystalline samples of UCr_2Al_{20} showed that the compound is a Pauli paramagnet at least down to the temperature of 1.7 K, as confirmed by featureless, metallic-like temperature variation of its specific heat and electrical resistivity. The absolute values of the nearly temperature-independent magnetic susceptibility of this uranium compound turned out to be of the order of those observed for its phonon reference – $ThCr_2Al_{20}$. It follows that the 5f electrons of uranium are unlikely to make a significant contribution to the magnetism of the former compound. However, they seem to make a noticeable contribution to the electron specific heat – the Sommerfeld coefficient in UCr_2Al_{20} was estimated to be about 80 mJ K^{-2}mol^{-1}, which is higher than $\gamma = 62$ mJ K^{-2}mol^{-1} found for the thorium compound (Swatek & Kaczorowski 2012). Swatek and Kaczorowski's findings on the magnetism of the UCr_2Al_{20} compound were confirmed by independent research (Matsumoto et al. 2013).

UMn_2Al_{20} Long-range ferromagnetic ordering in single crystals of the compound UMn_2Al_{20} was reported by Wang *et al* (Wang et al. 2010). The Curie temperature of the system was found to be around 20 K, which was inferred from the position of the phase transition anomaly in temperature variations of magnetization (distinct) and

specific heat (relatively small). Interestingly, no anomalies related to ferromagnetic ordering were observed in neutron scaterring spectra and electrical resistivity data. This interesting feature of UMn_2Al_{20} was interpreted by Wang *et al* as a manifestation of either heavy-fermion itinerant ferromagnetism with moderately small magnetic moment (leading to a reduction in the entropy change associated with the phase transition due to Kondo-type interactions) or singlet-triplet-induced local-moment ferromagnetism (Wang et al. 2010).

Later, Wiśniewski *et al* (Wiśniewski et al. 2012) confirmed the ferromagnetic phase transition in a high-quality UMn_2Al_{20} single crystal, but with a slightly smaller Curie temperature of 17.5 K, which was derived from an Arrot plot of the magnetization curves. To prove the spontaneous (rahter than field-induced) nature of the ferromagnetic ordering in the system, the single crystal was examined using polarized neutron scattering, which is much more sensitive to small magnetic moments than the usual neutron scattering method. Surprisingly, these experiments showed that the magnetism of UMn_2Al_{20} is due to the presence of magnetic moments at the sites of Mn atoms (with an ordered magnetic moment value of about $0.43\,\mu_B$/U), while the uranium sublattice remains non-magnetic (Wiśniewski et al. 2012).

UMo_2Al_{20}, UW_2Al_{20}, UTa_2Al_{20}, UNb_2Al_{20} UMo_2Al_{20} and UW_2Al_{20} in single-crystalline form were briefly described by Wang *et al* as Pauli paramagnets without any unusual features (Wang et al. 2010). The magnetic ground state of these two systems was later confirmed by Matsumoto *et al* (Matsumoto et al. 2013), based on magnetization measurements also made on single crystals. The existence of UTa_2Al_{20} was mentioned by Niemann and Jeitschko (Niemann & Jeitschko 1995a), but to the best of our knowledge, the results of its physical characterization have not been published to date. In turn, in the case of UNb_2Al_{20}, the crystal structure and basic physical properties were reported by Moussa *et al* (Moussa et al. 2017). The compounds was found to be paramagnetic at least down to 2 K and exhibit moderately enhanced electronic specific heat ($\gamma = 60\,\mathrm{mJ\,K^{-2}mol^{-1}}$).

1.3. Physical properties of UTE_2Al_{10}

UFe_2Al_{10} Magnetic properties of the compound UFe_2Al_{10} were first reported by Noël *et al* for a polycrystalline sample studied by DC magnetization and ^{57}Fe Mössbauer spectra measurements (Noël et al. 2004). The magnetization measurements showed that the compound remains paramagnetic at least down to 5 K, and its magnetic susceptibility can be described by the modified Curie-Weiss law with the fitting parameters $\mu_{\mathrm{eff}} = 2.62\,\mu_B$/U, $\theta_p = 107$ K and $\chi_0 = 4.87\times10^{-4}$ emu mol^{-1}. The ^{57}Fe Mössbauer spectroscopy revealed the presence of iron quadrupole doublets with the splitting $\Delta = 0.17\,\mathrm{mm\,s^{-1}}$ without further splitting at least down to 5 K, thus confirming the paramagnetic ground state of the compound. The room-temperature isomer shift relative to metallic iron, δ, was found to be unusually large as for Fe-Al containing

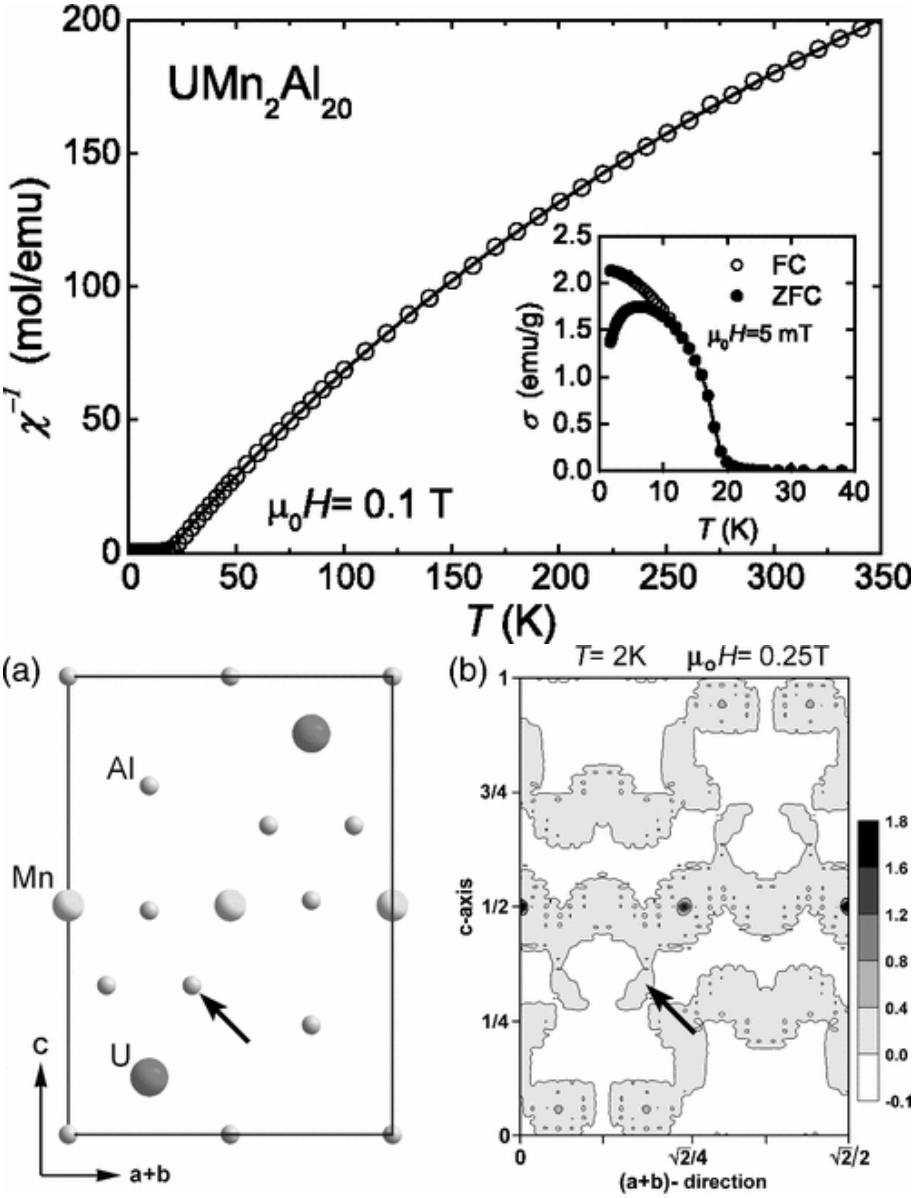

Figure 4. Magnetic properties (top) and map of magnetization density of UMn_2Al_{20} compared to its crystallographic unit cell (bottom). Reproduced with permission from (Wiśniewski et al. 2012).

intermetallics and equal to 0.29(1) mm s^{-1}. The lack of magnetic ordering down to 3 K was also mentioned by Halevy *et al* as a preliminary result of neutron diffraction experiments (Halevy et al. 2006).

Based on the results of high-pressure X-ray powder diffraction experiments carried out up to 23.5 GPa, the electron structure of UFe_2Al_{10} was calculated as a function of applied pressure, within the density functional theory (DFT) using the Linearised Augmented Plane Wave (LAPW) method and generalised gradient approximation (GGA) implemented in the WIEN97 code (Halevy et al. 2006). The uranium 5f states were found to remain localized in a narrow and well-defined band above the Fermi energy

E_F, while the iron 3d electron band – below E_F. The overlap between the U-5f and Fe-3d bands and the density of states (DOS) at E_F were found to be very small, suggesting a near-zero magnetic moment of uranium (Halevy et al. 2006). On the other hand, subsequent DOS calculations within DFT using the Full-Potential Linear Augmented Plane Waves (FP-LAPW) formalism with GGA, implemented in the WIEN2K code, showed that significant exchange splitting is expected to occur for the U-5f bands (Zenou et al. 2011). In particular, it was found that spin up states are shifted towards lower energy and cross E_F, while spin down states are shifted towards higher energy, exhibit a totally different DOS shape than spin up states, and show a visible drop of DOS below E_F (Zenou et al. 2011).

Studies of the physical properties of UFe_2Al_{10} carried out on a single-crystalline sample were first reported by Sugai *et al* (Sugai et al. 2011). The magnetic susceptibility measured in the [100] and [001] directions confirmed a clear Curie-Weiss behaviour of the compound above 150 K (with the effective magnetic moments of 3.13 μ_B/U and 3.14 μ_B/U, respectively), and no sign of magnetic ordering at least down to 2 K. For the [010] direction, the susceptibility was found to be small and almost independent of temperature. Interestingly, for all measured crystallographic orientations, the susceptibility appears to saturate as the temperature drops below 150 K, which has been attributed to the crystal field effect and the formation of a heavy-fermion state with a characteristic energy of about 100 K. The specific heat confirmed the lack of any magnetic ordering in UFe_2Al_{10} down to 0.4 K (Sugai et al. 2011).

Other studies on single crystals of the compound UFe_2Al_{10} were reported by Troć *et al* (Troć et al. 2015, Troć et al. 2017). They confirmed paramagnetic behaviour of the system down to 0.4 K with highly anisotropic magnetic susceptibility and, in addition, revealed anisotropic behaviour also in its electron-transport properties. It was shown that the system has metallic properties in general, describable by the fully delocalized electron model (*i.e.* including also delocalized 5f electrons of uranium). X-ray photoemission spectroscopy (XPS), interpreted using the results of fully relativistic DOS function calculations within DFT using the Full-Potential Local-Orbital (FPLO) code and Local Density Approximation (LDA), indicated the presence of U-5f bands in the valence spectra of UFe_2Al_{10} located close to E_F (in agreement with Halevy *et al* (Halevy et al. 2006)), thus supporting the *itinerant 5f states* scenario. However, a comparison of the photoemission spectra with those for UPd_3 and UNiSn (*i.e.* compounds commonly thought to have rather localized 5f electrons) and a closer look at the calculated DOS function revealed the possibility of partial localization of 5f electrons in UFe_2Al_{10}. The calculated Sommerfeld coefficient γ_b was found to be of about 27.2 mJ K^{-2}mol^{-1}, which is close to the experimental value γ_0 =28(1) mJ K^{-2}mol^{-1} estimated using specific heat data (Troć et al. 2015).

Furthermore, it was shown that the temperature dependence of the magnetic susceptibility, magnetoresistivity, thermoelectric power and heat capacity can be described in a consistent manner in terms of a crystal field (CF) model. In the case of UFe_2Al_{10}, the orthorhombic CF splits the $^3H_4$ ground multiplet of the U^{4+} ions

(with *localized 5f² electron shells*) into nine singlets, which characteristically modifies the aforementioned physical properties. These observations led Troć *et al* (Troć et al. 2015, Troć et al. 2017) to conclude that the 5f electrons in UFe_2Al_{10} are *dual* in nature (*i.e.* manifesting an itinerant character in some properties and a localized character in others) - a phenomenon predicted theoretically and discussed in detail *e.g.* in (Zwicknagl et al. 2002, Thalmeier 2002).

URu_2Al_{10} Physical properties of URu_2Al_{10} are similar to those of UFe_2Al_{10}. As shown by Troć *et al* (Troć et al. 2011), temperature variation of magnetic susceptibility of the former compound measured on a polycrystalline sample follows above 100 K the Curie-Weiss law with the fitting parameters $\mu_{\rm eff} = 3.36\,\mu_{\rm B}$/U and $\theta_{\rm p} = -169$ K. When the temperature is lowered, the susceptibility shows clear trend towards saturation, as observed in UFe_2Al_{10}. No magnetic ordering was found at least down to 2 K. Also electrical resistivity, magnetoresistivity and thermoelectric power show metallic-like behaviour with some characteristics of systems with crystal field interactions, yet the compound was discussed as a system with valence fluctuations (Troć et al. 2011).

Experiments carried out on a single-crystalline sample of URu_2Al_{10} (Sugai et al. 2011) revealed a highly anisotropic behaviour of its magnetic susceptibility and its qualitative similarity to that reported for UFe_2Al_{10}. In particular, they confirmed the Curie-Weiss behaviour of the susceptibility above 150 K for the [100] and [001] directions (with the effective magnetic moments of $3.50\,\mu_{\rm B}$/U and $3.07\,\mu_{\rm B}$/U, respectively), and no sign of magnetic ordering at least down to 2 K. And, as in the Fe-containing phase, for the [010] direction the susceptibility was found to be small and almost independent of temperature.

XPS measurements and fully relativistic FPLO-LDA band structure calculations reported by Samsel-Czekała *et al* (Samsel-Czekała et al. 2013) showed that, as in UFe_2Al_{10}, the U-5f bands in URu_2Al_{10} are located near $E_{\rm F}$ and are probably strongly hybridized with the 4d electrons of ruthenium, suggesting *itinerant* character of the uranium 5f electrons in this compound. Here, the calculated Sommerfeld coefficient $\gamma_{\rm b}$ is equal to 21.5 mJ K^{-2}mol^{-1} and is close to the experimental value 22 mJ K^{-2}mol^{-1} derived from the specific heat data.

The results of magnetic properties measurements carried out on single-crystalline samples of URu_2Al_{10} reported by Troć *et al* (Troć et al. 2018) confirmed the findings of Sugai *et al* (Sugai et al. 2011). In particular, they showed highly anisotropic magnetic susceptibility with Curie-Weiss behaviour at elevated temperature and almost temperature-independent susceptibility at low temperature. Both the temperature dependence of the magnetic susceptibility of the single crystals of URu_2Al_{10} and their specific heat, electrical resistivity and thermoelectric power were successfully described using a crystal field model applied to U^{4+} ions (with $5f^2$ electron configuration), as was done previously for UFe_2Al_{10} (Troć et al. 2015). This was also considered in this case as evidence of *partial localization of the 5f electrons* of uranium.

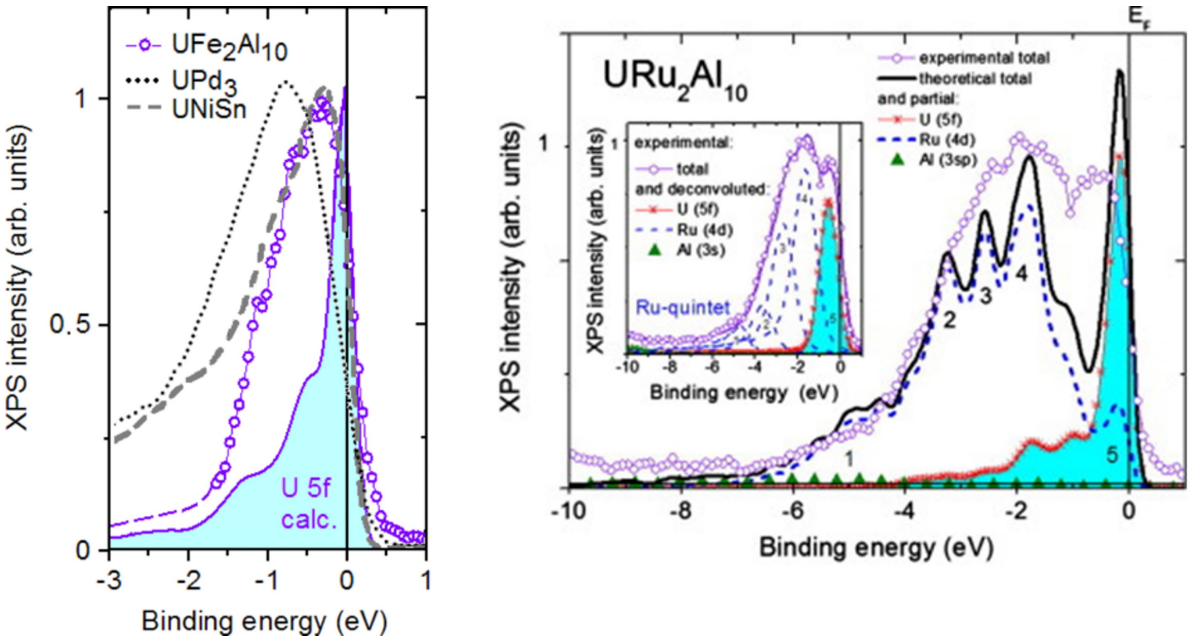

Figure 5. The experimental and calculated U-5f spectra of UFe_2Al_{10} (left) and URu_2Al_{10} (right). The former is compared with the spectra of UPd_3 and UNiSn, and the latter is supplemented by the respective contributions of the constituent elements to the total DOS. Reproduced with permission from (Troć et al. 2015) and (Samsel-Czekała et al. 2013).

UOs_2Al_{10} The paramagnetic behaviour of another 1:2:10 phase with uranium, namely UOs_2Al_{10}, was briefly mentioned by Sugai *et al* (Sugai et al. 2011), but without showing experimental data. The results of a systematic study of the compound UOs_2Al_{10} were only first reported by Troć *et al* (Troć et al. 2019)

The magnetic susceptibility of UOs_2Al_{10} is strongly anisotropic, with the [100] and [001] axes showing the Curie-Weiss behaviour of $\chi^{-1}(T)$ above about 100–150 K (with the effective magnetic moment of 2.88 μ_B/U and 2.89 μ_B/U, respectively), and the [010] direction showing a strongly curvilinear $\chi^{-1}(T)$. That strongly anisotropic temperature dependence of the susceptibility measured in each direction has been successfully described within the crystal field model, assuming the presence of the U^{4+} ions with the $5f^2$ configuration, *i.e. localized* 5f electrons. The influence of the crystal field effect has been recognised by Troć *et al* (Troć et al. 2019) also in transport properties and specific heat of the compound described.

In turn, fully relativistic FPLO-LDA band structure calculations showed the possibility of relatively broad U-5f electron bands just below the Fermi level, resembling those calculated for the Fe counterpart, indicating the metallic nature of UOs_2Al_{10}. The calculated Sommerfeld coefficient $\gamma_b = 18.9\,\mathrm{mJ\,K^{-2}mol^{-1}}$ is close to the experimental value $\gamma(0) = 25.9\,\mathrm{mJ\,K^{-2}mol^{-1}}$ estimated using specific heat data. This led the authors (Troć et al. 2019) to the conclusion about the *dual* nature of the 5f electrons, similar to that of UFe_2Al_{10} and URu_2Al_{10}.

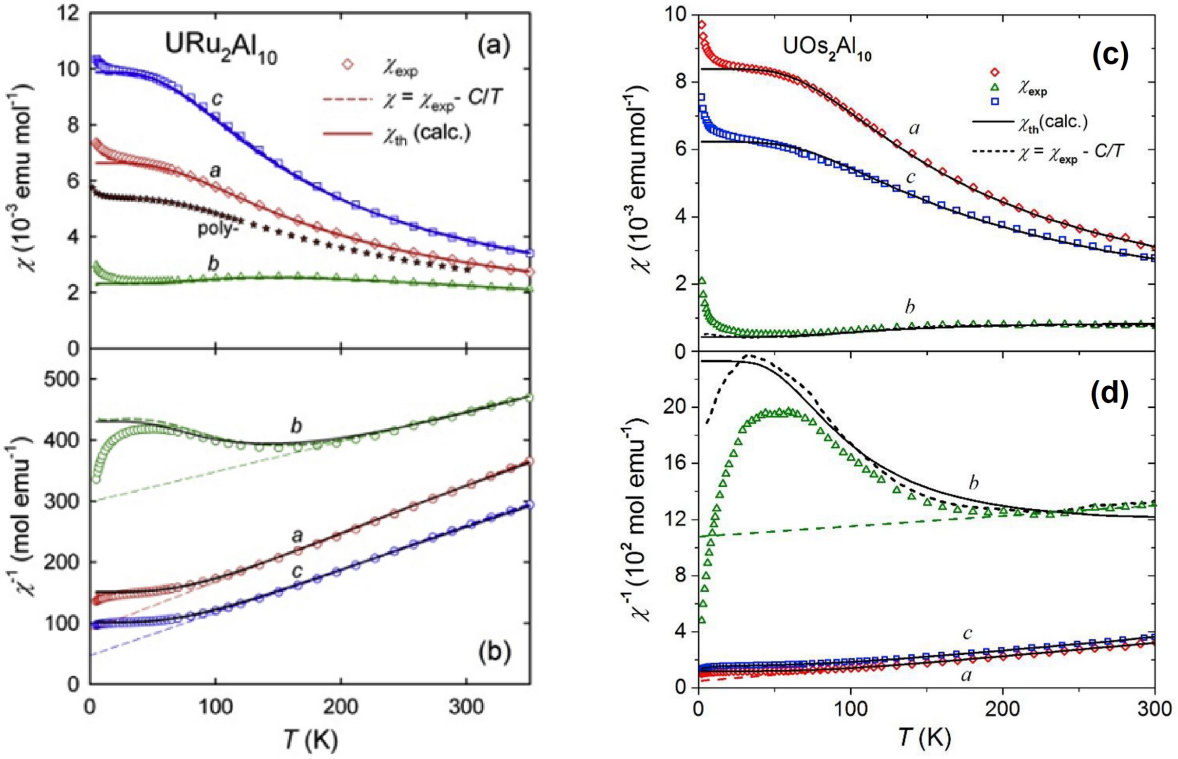

Figure 6. Magnetic susceptibility (up) and its inverse (down) of single crystalline URu_2Al_{10} (a,b) and UOs_2Al_{10} (c,d) measured along the three crystallographic axes of the orthorhombic unit cell. The symbols are experimental values and the solid lines fits using crystal field models. Reproduced with permission from (Troć et al. 2018) and (Troć et al. 2019).

2. Shastry-Sutherland-like lattice in $U_6TE_4Al_{43}$

2.1. Crystal structure of $U_6TE_4Al_{43}$

Crystal structure of compounds in the $U_6TE_4Al_{43}$ family represents an intermediate configuration between the other two described in this review article (*i.e.* UTE_2Al_{10}/UTE_2Al_{20} and $U_3TE_4Al_{12}$). They crystallize within a hexagonal structure of the $Ho_6Mo_4Al_{43}$ type (space group $P6_3/mmc$, no. 194).

In this structure type, on the one hand, the f-electron magnetic atoms form dumbbells with interatomic spacing of about 3.5 Å, aligned – with a slight angle of inclination – along the c-axis and separated the one from the other by distances slightly greater than 5 Å, both along the c-axis and in the ab-plane. On the other hand, these dumbbells are embedded in cages resembling "peanuts", in which distances between the f-electron atoms and ligands (*e.g.* ranging from 3.081 to 3.408 Å in $U_6Mo_{4+x}Al_{43-x}$ (Noël et al. 2009)) are larger than the sum of the metallic radii of the constituent elements.

Such a characteristic arrangement of magnetic atoms resembles the so-called planar Shastry-Sutherland lattice (Shastry & Sutherland 1981). A non-trivial set of interactions

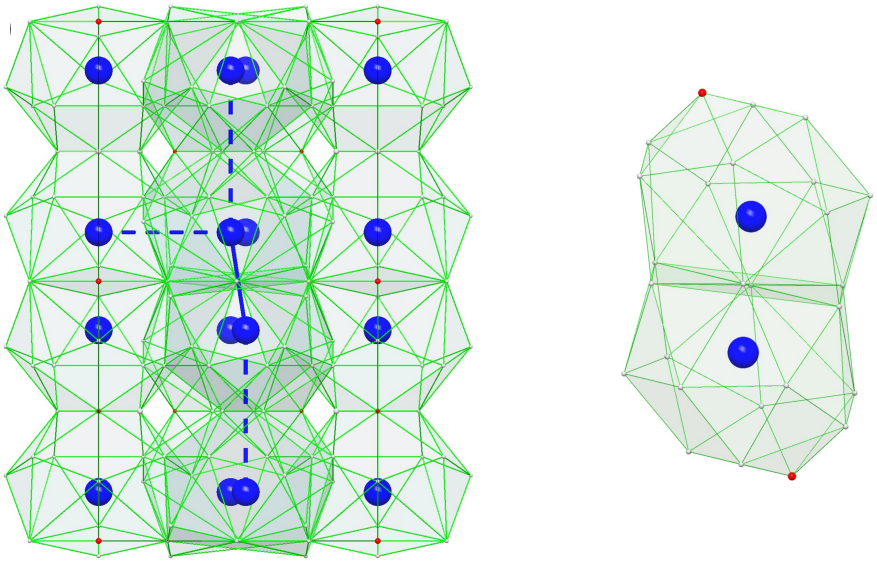

Figure 7. Crystal structures of $U_6TE_4Al_{43}$ (left) together with coordination polyhedra around U dimer showing a "peanut"-shape cage (right). U atoms are shown as large blue spheres, TE-atoms in red, and Al in grey. U-U distances close to 3.5 Å are shown as solid blue lines and those above 5 Å as dashed blue lines.

between magnetic moments and their nearest neighbors makes such crystal structures a source of magnetic frustration, or at least complex magnetic behavior. The systems U_2TE_2X crystallizing with a tetragonal structure of the Mo_2FeB_2 type exhibit this configuration of uranium atoms, which leads to their complex magnetic ordering (see *e.g.* U_2Pd_2In (Prokeš et al. 2020)).

Although such 6-4-43 phases were discovered almost 30 years ago by Niemann and Jeitschko for uranium aluminides with 6 transition elements from the columns VB and VIB of the periodic table (Niemann & Jeitschko 1995a), only two reports on basic physical properties of $U_6Nb_4Al_{43}$ and $U_6W_4Al_{43}$ have been published to date.

2.2. Physical properties of $U_6TE_4Al_{43}$

$U_6Nb_4Al_{43}$ According to Moussa *et al* (Moussa et al. 2017), who studied polycrystalline samples of $U_6Nb_4Al_{43}$, the compound shows at high temperatures a Curie-like paramagnetic behavior with $\mu_{\text{eff}} = 2.38\,\mu_B/\text{U}$, $\theta_p = -134(1)\,\text{K}$ and Pauli-like contribution $\chi_0 = 8.02(7)\times10^{-4}\,\text{emu}\,\text{mol}_U^{-1}$ (fig. 8a). At low temperature the system exhibits at least 2 magnetic phase transitions. The first of these was detected in the temperature dependence of magnetic susceptibility at about 12 K, and was visible as a cusp whose shape was almost independent of the applied magnetic field (Fig. 8c). Therefore, it was interpreted as a manifestation of some kind of AFM order. The second magnetic transition occurred in the magnetic susceptibility at about 8 K, had a shape resembling a Brillouin anomaly with a distinct magnetic hysteresis, and was very sensitive on external magnetic field (Fig. 8c). Hence, it was interpreted by the authors as a manifestation of FM ordering.

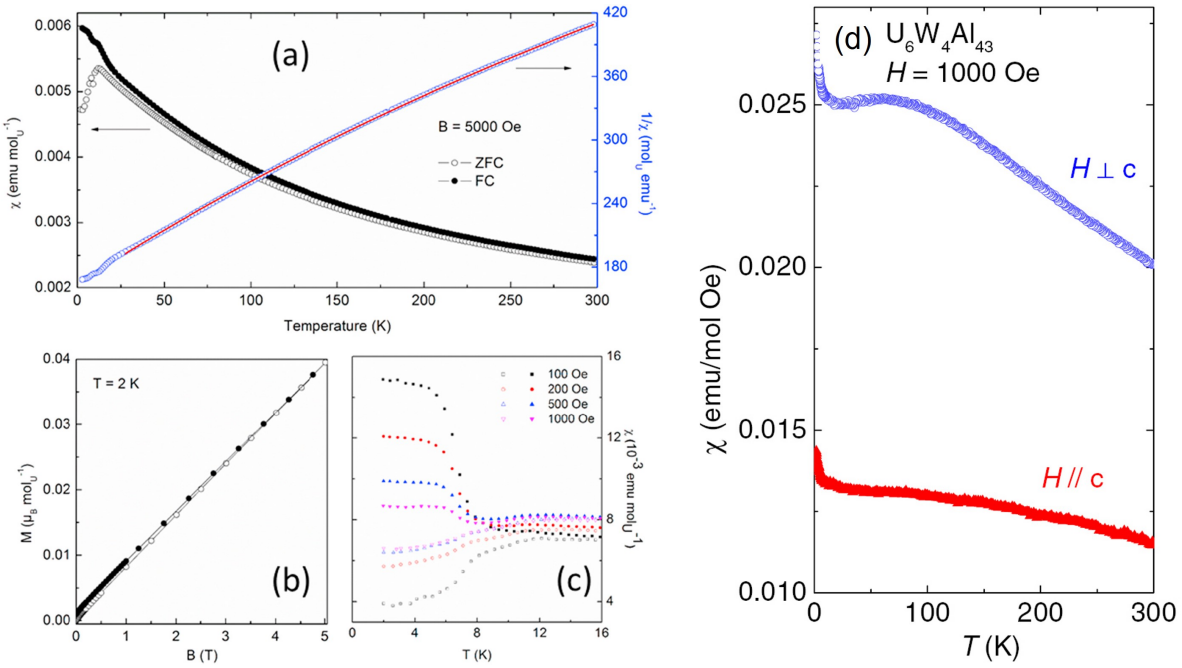

Figure 8. Magnetic properties of polycrystalline $U_6Nb_4Al_{43}$ (a-c) and single crystalline $U_6W_4Al_{43}$ (d). Reproduced with permission from (Moussa et al. 2017) and (Huang et al. 2019).

Temperature variations of the specific heat and electrical resistivity of $U_6Nb_4Al_{43}$ showed only single, broad anomalies below about 12 K with some sharp drop of the resistivity below 8 K, confirming the intrinsic nature of the observed transitions. The electrical resistivity below 8 K was described in terms of the Fermi liquid scenario in the presence of AFM spin waves with a gap in magnon spectra of about 39 K. In turn, the Sommerfeld coefficient of the compound was found to be moderately enhanced ($\gamma = 133\,\mathrm{mJ\,K^{-2}mol_U^{-1}}$), which was interpreted as a manifestation of strong electron correlations.

$U_6W_4Al_{43}$ As reported by Huang *et al* (Huang et al. 2019), no magnetic ordering was observed in $U_6W_4Al_{43}$ at least down to 2 K (Fig. 8(d)) and the effective magnetic moment estimated from the high-temperature magnetic susceptibility was about 1.8-2.0 μ_B/U, much more reduced than in other compounds described here. The temperature variation of the electrical resistivity of $U_6W_4Al_{43}$ showed a negative slope followed, by a maximum at low temperature. This was interpreted by the authors as possibly indicating the presence of Kondo-like interactions in the compound, similarly to the resistivity of UTE_2Al_{10} or U_2RuGa_8 (Troć et al. 2015, Troć et al. 2018, Troć et al. 2005). The Sommerfeld coefficient of the $U_6W_4Al_{43}$ phase turned out to be about half that reported for $U_6Nb_4Al_{43}$ (70 vs. 133 $\mathrm{mJ\,K^{-2}\,mol_U^{-1}}$), hinting at much weaker electron interactions.

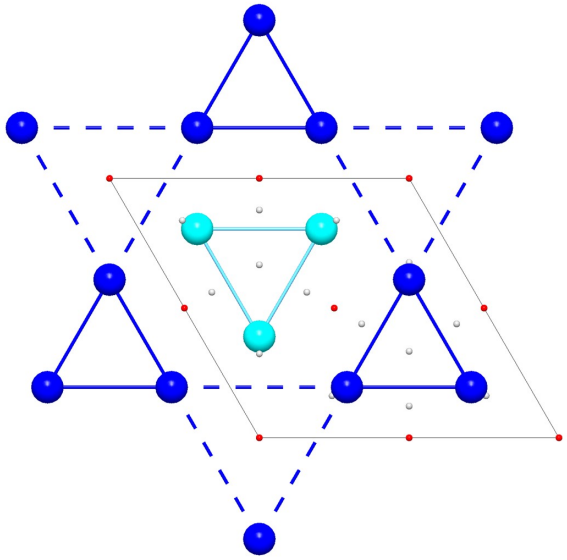

Figure 9. Crystal structure of $U_3TE_4Al_{12}$ projected along the c-axis and highlighting the breathing kagome network formed by U-atoms.

3. *Breathing* kagome lattice in $U_3TE_4Al_{12}$

3.1. Crystal structure of $U_3TE_4Al_{12}$

The compounds with stoichiometry $U_3TE_4Al_{12}$ have been reported for TE denoting iron (Gonçalves et al. 2009), cobalt (Tougait et al. 2004, Tougait et al. 2007) and ruthenium (Pasturel et al. 2009, Troć et al. 2012, Gorbunov et al. 2019, Asaba et al. 2020). They all crystallize with a hexagonal structure of the $Gd_3Ru_4Al_{12}$ type (space group $P6_3/mmc$, no. 194), which is an ordered derivative of the $EuMg_{5.2}$ type structure (Gladyshevskii et al. 1993). It is a result of the stacking of planar [U,Ge] layers intercalated with layers made of TE-centered chair-like [Al6] hexagons. *Ab initio* calculations confirmed the stability of these phases, often enhanced by preferential substitution of Al by TE-atoms at *6h* sites (Chen et al. 2010).

Unlike the previous families, the uranium-atoms in the $U_3TE_4Al_{12}$ compounds are neither isolated from each other nor caged. Indeed, on the one hand, the shorter U-Al interatomic distances ($d \approx 2.9 \div 3.0$ Å) are close to the sum of the corresponding metallic radii ($r_U + r_{Al} \approx 2.99$ Å). On the other hand, the uranium sublattice has been described as a distorted kagome lattice with small [U3] triangles ($d_{U-U} \approx 3.5$ Å) being connected the one to each other via much larger ones ($d_{U-U} > 5$ Å). It can also be noticed that the U-U distance between two adjacent layers is larger than 5 Å. Magnetic interactions between U-atoms are therefore expected to be much stronger within the small uranium triangles than within the large ones or between the layers.

The distribution of uranium atoms in such breathing kagome lattices is crucial for the aforementioned competition of magnetic interactions, which can lead to *i.e.*

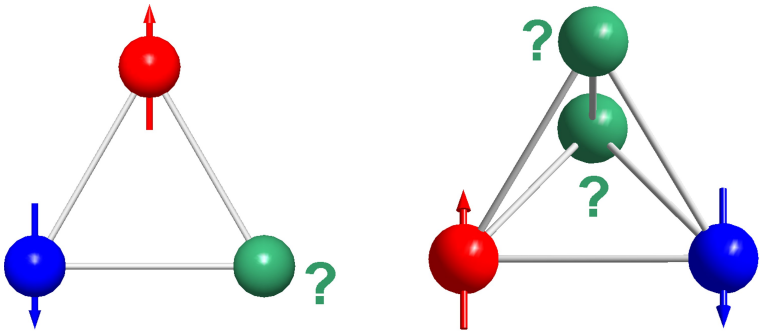

Figure 10. Scheme illustrating the impossibility to align all the magnetic moments in a perfect antiferromagnetic order in triangular or tetrahedral lattices.

the opening of a band gap at the Fermi level (if considered from reciprocal space), or to magnetic frustration (if viewed rather from the point of view of direct space). The opening of the gap can then lead to certain topological insulating properties or skyrmion phases (Tokura et al. 2019, Hirschberger et al. 2019, Swain et al. 2022), while frustration often leads to spin-glass, spin-liquid, and related behavior, or at least complex magnetic ordering. Understanding the mechanisms of these phenomena observed in solids is currently quite a hot topic for physicists and explains to a large extent their strong interest in the compounds crystallizing is the $Gd_3Ru_4Al_{12}$ type structure (Ogunbunmi et al. 2022).

As for magnetic frustration and complex magnetic ordering, so far the most studied origin of these phenomena is indeed some unique arrangement of magnetic atoms. In particular, as shown in Fig. 10, it is impossible to align magnetic moments in perfect antiferromagnetic order in, for example, a triangular or tetrahedral lattice (Balents 2010). To lower the energy of such a system, the magnetic moments adopt an orientation intermediate between the energetically favorable antiferromagnetic (AFM) state and the unfavorable ferromagnetic (FM) state. The pyrochlore lattice is a canonical example of such a frustrated system (Gingras & McClarty 2014, Lhotel et al. 2020, Reig-i-Plessis & Hallas 2021). Another origin of the magnetic frustration occurs when a magnetic atom undergoes several different interactions with its nearest neighbors. This is the case of the planar Shastry-Sutherland lattice, discussed in Sec. 2.

In turn, a wide range of more or less complex AFM or FM magnetic orderings have been observed for compounds based on rare earth elements, as reviewed in detail by Ogunbunmi *et al* (Ogunbunmi et al. 2022). As an example, Nakamura *et al* wrote about the RKKY interaction-driven formation of FM magnetic trimers in the prototype aluminide $Gd_3Ru_4Al_{12}$, (Nakamura et al. 2018). Below we focus on physical properties of the uranium-based compounds from that family, namely $U_3TE_4Al_{12}$ (where TE = Fe, Co and Ru).

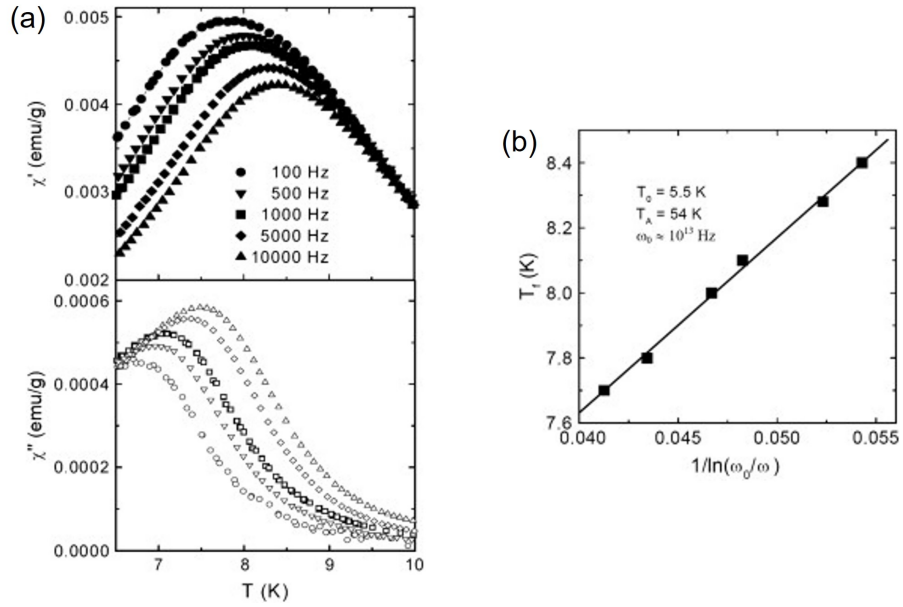

Figure 11. (a) AC magnetic susceptibility of $U_3Fe_{4+x}Al_{12-x}$ as a function of temperature, measured with various frequencies of the probing magnetic field. (b) Vogel-Fulcher plot of freezing temperature T_f vs. frequency ω of the probing magnetic field. Reproduced with permission from (Gonçalves et al. 2009).

3.2. Physical properties of $U_3TE_4Al_{12}$

$U_3Fe_4Al_{12}$ As expected from its crystal structure, magnetic properties of the $U_3Fe_{4+x}Al_{12-x}$ phase show some features characteristic of spin-glass (SG) systems. In particular, a broad cusp with a maximum at so-called freezing temperature T_f of about 8 K (Fig. 11(a)) with a distinct and very characteristic dependence of its position on the frequency of the probing magnetic field (Fig. 11(b)) was observed by Gonçalves *et al* (Gonçalves et al. 2009) in AC magnetic susceptibility of a polycrystalline sample of that compound. The long-range ordering did not take place despite the finding of an antiferromagnetic interaction between magnetic moments of uranium ions ($\mu_{\text{eff}} = 3.54(1)\,\mu_B$/U, $\theta_p = -25.5(1)$ K). ^{57}Fe Mössbauer spectroscopy, on the other hand, showed that the origin of the SG behavior is not related to the Fe sublattice and should therefore be considered as a consequence of topological frustration of the uranium magnetic moments.

Ab initio calculations of the phonon spectra of the $U_3Fe_4Al_{12}$ phase showed that Al atoms contribute predominantly to vibrational modes in the high-freqeuency region ($\approx 4 \div 11$ THz), Fe atoms contribute heavily to modes with lower frequencies (mainly between about 1 and 6 THz) while U atoms contribute only to the modes below 4.00 THz (Chen et al. 2010).

$U_3Co_4Al_{12}$ $U_3Co_{4+x}Al_{12-x}$ was found to exhibit similar SG-like features as the phase with Fe. As reported by Tougait *et al* (Tougait et al. 2004), DC magnetic susceptibility

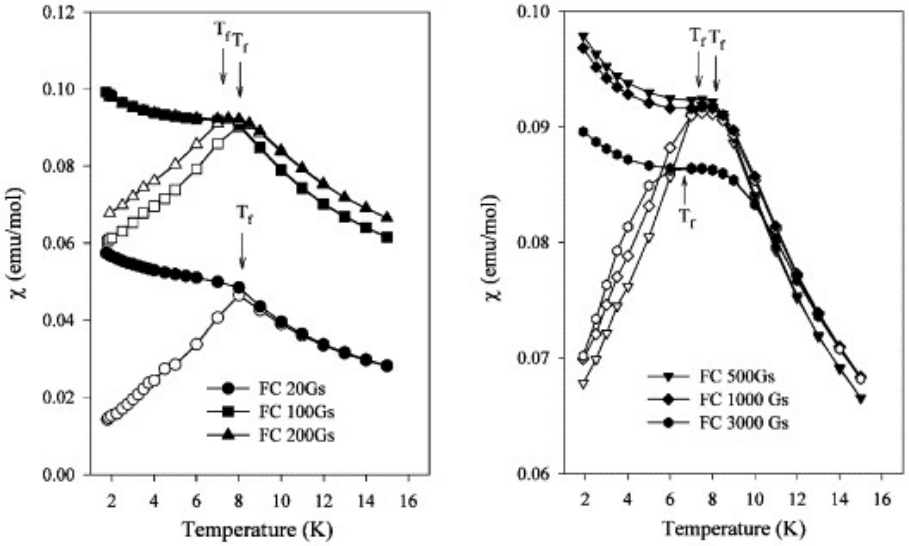

Figure 12. DC magnetic susceptibility of $U_3Co_{4+x}Al_{12-x}$ as a function of temperature, measured in various external magnetic fields. Reproduced with permission from (Tougait et al. 2004).

of the compound with $x = 0.55$ shows an AFM-like cusp at about 8 K, but with a large difference below that temperature between the magnetization curves measured in zero and non-zero magnetic fields (Fig. 12). Such magnetization behavior rules out long-range antiferromagnetic ordering and clearly indicates the freezing of magnetic moments of uranium in a rather random orientation. It is worth noting that the effective magnetic moment of uranium in the phase with Co ($\mu_{\text{eff}} = 2.70(1)\,\mu_{\text{B}}/\text{U}$) is somewhat smaller than in the phase with Fe. Also, the estimated paramagnetic Curie-Weiss temperature ($\theta_{\text{p}} = -10(1)\,\text{K}$) is smaller (in absolute values) than in $U_3Fe_{4+x}Al_{12-x}$.

The SG behavior in $U_3Co_{4+x}Al_{12-x}$ was later confirmed by the same research group with measurements of AC magnetic susceptibility, specific heat and electrical resistivity. These experiments showed a pronounced isothermal logarithmic relaxation of the compound remnant magnetization with a time constant τ of slightly more than 200 minutes (Fig. 13(a)), a characteristic frequency dependence of the freezing temperature, consistent with Shrtikman and Wohlfarth's predictions (Shtrikman & Wohlfarth 1981) (Fig. 13(b)), and the absence of any anomalies at T_{f} in the temperature variation of the compound specific heat and electrical resistivity.

By analogy with the results of the SG behavior in URh_2Ge_2, reported by Süllow *et al* (Süllow et al. 1997), the SG behavior in the $U_3Co_{4+x}Al_{12-x}$ system was attributed by the authors (Tougait et al. 2007) to multiple possible configurations of perturbations of magnetic moments separated by barriers of different heights.

$U_3Ru_4Al_{12}$ Given the SG properties of the Fe- and Co-based uranium aluminides, the occurence of the AFM transition at $T_{\text{N}} = 8.4\,\text{K}$ in a polycrystalline sample of $U_3Ru_4Al_{12}$ was surprising at first glance (Pasturel et al. 2009). The ability to grow single crystals

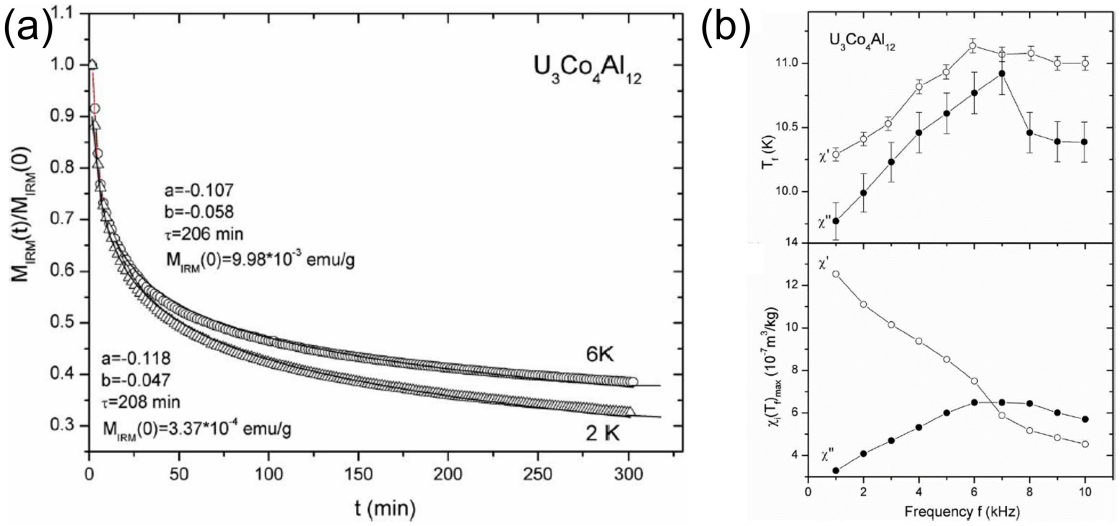

Figure 13. (a) Time dependence of isothermal remnant magnetization of $U_3Co_{4+x}Al_{12-x}$. (b) Vogel-Fulcher plot of freezing temperature T_f vs. frequency f of the probing magnetic field. Reproduced with permission from (Tougait et al. 2007).

of this compound using the Czochralski pulling method made it possible to study its physical properties in greater depth (Troć et al. 2012).

DC magnetization measurements carried out on the so-obtained single crystals of the compound $U_3Ru_4Al_{12}$ showed noticeable magnetocrystalline anisotropy and that the *a*-axis is the easy one (Fig. 14(a)). The effective magnetic moment μ_{eff} was found to be markedly reduced ($2.72\,\mu_B$/U for the *a*-axis and $2.45\,\mu_B$/U for the *c*-axis), as in $U_3Co_4Al_{12}$. The paramagnetic Curie-Weiss temperature θ_p was estimated as being of about $-19.1(3)$ K and $-40.5(3)$ K, respectively, indicating the dominant antiferromagnetic interactions between the uranium magnetic moments (Troć et al. 2012). Neutron diffraction experiments confirmed the long-range ordering of the uranium magnetic moments in the basal *ab*-plane, *i.e.* the breathing kagome lattice, with a noncollinear arrangement leading to a global moderate FM component in these planes. The latter are stacked antiferromagnetically along the *c*-axis (Fig. 14(b)), resulting in the global AFM character of the $U_3Ru_4Al_{12}$ compound (Troć et al. 2012).

It is worth noting that the postulated magnetocrystalline anisotropy was much more pronounced in the electrical transport properties of the system, namely the electrical resistivity and Seebeck coefficient (Troć et al. 2012). Their temperature variations, along with a moderately enhanced electron contribution to the specific heat, were interpreted by Troć *et al* as manifestation of the Kondo and crystal field effects in this ternary aluminide.

Measurements of magnetization and sound velocity made in magnetic fields up to 60 T by Gorbunov *et al* (Gorbunov et al. 2019) allowed the construction of the magnetic phase diagram of $U_3Ru_4Al_{12}$ (Fig. 14c). The experiments revealed the existence of 3 magnetically ordered phases below T_N when the magnetic field H is applied along

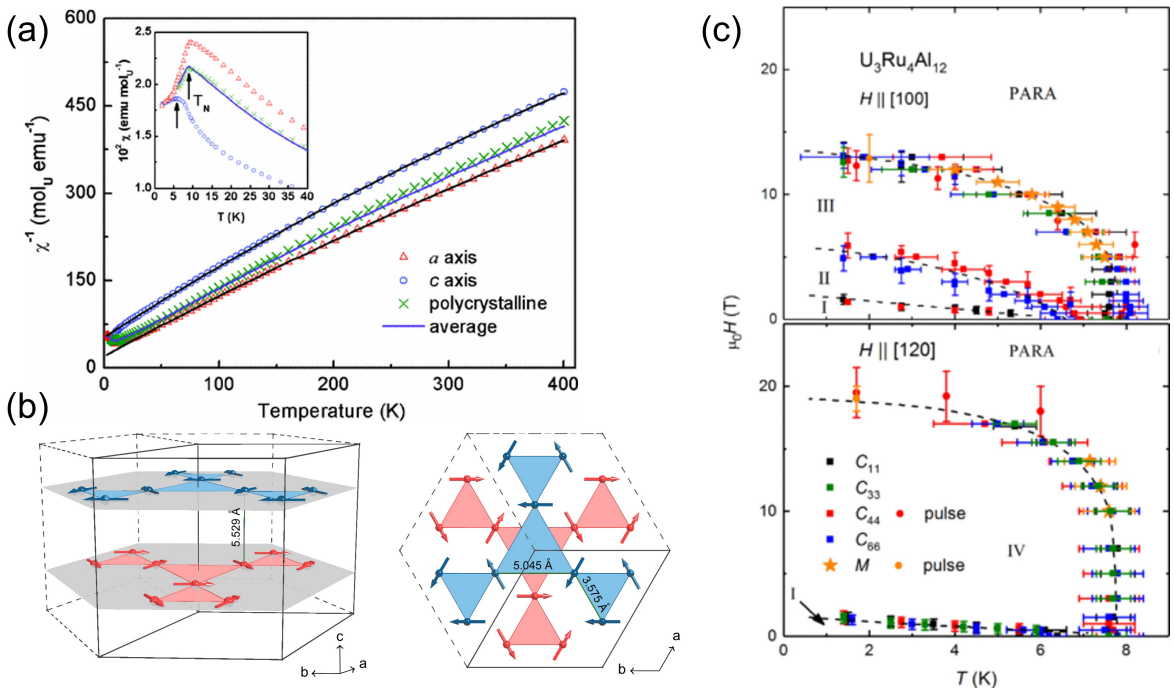

Figure 14. (a) DC magnetization of $U_3Ru_4Al_{12}$ measured as a function of temperature. (b) Magnetic structure in zero magnetic field determined from neutron diffraction experiment. (c) Magnetic phase diagram obtained from measurements of magnetic and elastic properties made in high magnetic fields. Reproduced with permission from (Troć et al. 2012) and (Gorbunov et al. 2019).

the a-axis (*i.e.* [100]), and 2 phases for $H|||[120]$. Crystal field analysis reproduces the experimental magnetization data relatively well, leading to the conclusion that quadrupolar interactions cause a pronounced elastic softening of the C_{44} shear modulus.

Finally, a non-linear variation of the anomalous Hall effect of $U_3Ru_4Al_{12}$ with the magnetic field, together with a strong angular dependence of that intrinsic property, was demonstrated by Asaba *et al* (Asaba et al. 2020). They associated the observed behavior to the nonlinear response of the Berry's curvature, and thus demonstrated that a heavy fermion noncollinear antiferromagnet can be driven into a regime with a nonlinear response of the Berry curvature. This discovery opens up the possibility of tuning the topological properties of such heavy-fermion systems using magnetic fields.

4. Discussion and Concluding remarks

This review describes four families of Al-rich ternary uranium compounds: (i) UTE_2Al_{20}, (ii) UTE_2Al_{10}, (iii) $U_6TE_4Al_{43}$, and (iv) $U_3TE_4Al_{12}$. U-atoms in the first two groups of compounds, namely UTE_2Al_{20} and UTE_2Al_{10}, are embedded in rather large cages formed by TE- and/or Al-atoms, and are separated the one from the others by distances greater than 5 Å (Fig. 1). The $5f$ magnetic atoms are therefore well isolated, so these compounds can be considered as *zero-neighbor systems*. Indeed, none of these

aluminides order magnetically, except for UMn_2Al_{20} due to the Mn-sublattice. Curie-like paramagnetism in the presence of crystal-field effect are mainly dominating their physical properties.

The next two families of compounds described here, namely $U_6TE_4Al_{43}$ and $U_3TE_4Al_{12}$ could be considered as *one-neighbor* and *two-neighbor* systems, respectively, due to the formation of characteristic U-dimers (in the Shastry-Sutherland lattice (Shastry & Sutherland 1981)) and U-triangles (in the breathing kagome lattice (Gladyshevskii et al. 1993)) with U-U distances close to the Hill limit (about 3.5 Å). These objects (dimers or triangles) are then separated one from the other by more than 5 Å, forming perfect lattices for the occurrence of magnetic frustration of different origins.

The 6-4-43 phases are the least studied of the three groups of compounds described in this review. While several $RE_6TE_4Al_{43}$ are described in the literature, only the physical properties of two U-based phases, namely $U_6W_4Al_{43}$ and $U_6Nb_4Al_{43}$, have been reported so far. Since these two compounds exhibit a significantly different magnetic ground state (paramagnetic for W vs. complex magnetic order for Nb), it is of utmost importance to study the 4 other members of this family, preferably using single crystals. In this context, it is worth noting that we have recently used the narrow temperature range in which $U_6Nb_4Al_{43}$ is in equilibrium with Al (Moussa et al. 2017) to grow such crystals using the flux method, and preliminary results indicate a strong anisotropy of physical properties of this compound.

A quick look at reports on the physical properties of isostuctural rare earth-based aluminides corroborates the possibility of multiple magnetic transition driven by the particular geometry of the magnetic atom sublattice (Wolff et al. 2001, Verbovytsky Yu et al. 2008, Kangas et al. 2013, Maurya et al. 2014, Treadwell et al. 2014). In the case of $Tm_6Cr_4Al_{43}$, Fushiya *et al* suggest the possibility of magnetic dimer formation, though measurements at lower temperatures are needed to prove this hypothesis (Fushiya et al. 2014). Moreover, superconductivity has been observed below 1 K in the isostructural phases $Y_6TE_4Al_{43}$ for TE = Nb, Mo, Ta (Kase et al. 2016). Although their uranium-based counterparts with Nb and W do not show such a transition, it seems reasonable to examine in this regard a hypothetical non-magnetic series with Th, *i.e.* $Th_6TE_4Al_{43}$.

The striking structural feature of the $U_3TE_4Al_{12}$ compounds (*i.e.* the breathing kagome lattice formed by uranium atoms) has probably a huge impact on the physical properties of these compounds, since two of them (with TE = Fe, Co) show SG-like features, and only one (with TE = Ru) shows long-range (but complex) AFM order. The impressive range of exotic physical phenomena observed in the kagome lattices and their possible applications (see *e.g.* (Yağcı 2021) are a strong argument for the search for new actinide-based members from this family and further investigations of their properties on single-crystalline specimens.

Significantly, most of the theoretical calculations carried out for the $Gd_3Ru_4Al_{12}$-type compounds, both with rare earths and actinides, consider only magnetic

interactions within the breathing kagome lattice. However, it is worth noting that the U-U (or *RE-RE*) distances within the the large triangles of such a lattice (just over 5 Å) are very similar to the U-U distances between two consecutive planes along the *c*-axis. In our opinion, this additional complexity cannot be ignored when considering the physical properties and trying to understand the underlying microscopic mechanisms.

In conclusion, the four families of uranium aluminides described in this review certainly provide a unique playground for physicists to better understand the magnetic interactions between U magnetic moments while gradually increasing the number of their nearest magnetic neighbors. Moreover, the physical properties of the 3-4-12 and 6-4-43 series are more or less clearly influenced by the geometry of their crystal lattice, which promotes the occurrence of magnetic frustration. The various ground states of their members can therefore be helpful in understanding the fundamental origins of magnetic freezing phenomena.

References

Andreev A V, Shiokawa Y, Tomida M, Homma Y, Sechovsky V, Mushnikov N V & Goto T 1999 J. Phys. Soc. Jpn. **68**, 2426–2432.
URL: *https://journals.jps.jp/doi/10.1143/JPSJ.68.2426*

Asaba T, Su Y, Janoschek M, Thompson J D, Thomas S M, Bauer E D, Lin S Z & Ronning F 2020 Phys. Rev. B **102**, 035127.
URL: *https://journals.aps.org/prb/abstract/10.1103/PhysRevB.102.035127*

Balents L 2010 Nature **464**, 199–208.
URL: *https://www.nature.com/articles/nature08917*

Chen Y, Shen J & Chen N 2010 J. Solid State Chem. **183**, 504–509.
URL: *https://www.sciencedirect.com/science/article/pii/S0022459609005945*

Clement Ravi Chandar S, Venkiteswaran C N, Divakar R, Naga Sivayya D, Sengupta A K, Agarwal R & Kamath H S 2020 Vol. 5 Elsevier pp. 102–138.
URL: *ttps://www.sciencedirect.com/science/article/pii/B9780128035818117837*

Dienst W, Nazaré S, & Thümmler F 1977 J. Nucl. Mater. **64**, 1–13.
URL: *https://www.sciencedirect.com/science/article/pii/0022311577900022*

Durand J P & Laudamy P 1994 in 'Proceedings of the 1994 International Meeting on Reduced Enrichment for Research and Test Reactors' Argonne National Laboratory Williamsburg, Virginia, USA.

Durazzo M, Conturbia G L C R & Urano de Carvalho E F 2021 Prog. Nucl. Energ. **140**, 103920.
URL: *https://www.sciencedirect.com/science/article/pii/S0149197021002808*

Fushiya K, Miyazaki R, Higashinaka R, Matsuda T D & Aoki Y 2014 JPS Conf. Proc. **3**, 011018.
URL: *https://journals.jps.jp/doi/abs/10.7566/JPSCP.3.011018*

Geibel C, Ahlheim U, Giorgi A L, Sparn G, Spille H, Steglich F & Suski W 1990 Physica B **163**, 194–196.
URL: *https://www.sciencedirect.com/science/article/pii/092145269090166R*

Ghosh T, Dutta M, Sarkar D & Biswas K 2022 J. Am. Chem. Soc. **144**, 10099–10118.
URL: *https://pubs.acs.org/doi/10.1021/jacs.2c02017*

Gingras M J P & McClarty P A 2014 Rep. Prog. Phys. **77**, 056501.
URL: *https://iopscience.iop.org/article/10.1088/0034-4885/77/5/056501*

Gladyshevskii R E, Strusievicz O R, Cenzual K & Parthé E 1993 Acta Crystallogr. B-Structural Science **49**, 474–478.
URL: *http://scripts.iucr.org/cgi-bin/paper?S0108768192011510*

Gonçalves A & Noël H 2005 Intermetallics **13**, 580–585.
URL: *https://www.sciencedirect.com/science/article/pii/S0966979504003152*

Gonçalves A P, Waerenborgh J C, Gaczyński P, Noël H & Tougait O 2009 Intermetallics **17**, 25–31.
URL: *https://www.sciencedirect.com/science/article/pii/S0966979508001933*

Gorbunov D, Ishii I, Nomura T, Henriques M, Andreev A, Uhlarz M, Suzuki T, Zherlitsyn S & Wosnitza J 2019 Phys. Rev. B **99**, 054413.
URL: *https://journals.aps.org/prb/abstract/10.1103/PhysRevB.99.054413*

Halevy I, Sterer E, Aizenshtein M, Kimmel G, Regev D, Yahel E, Pereira L C J & Gonçalves A P 2001 Journal of Alloys and Compounds **319**(1), 19–21.
URL: *https://www.sciencedirect.com/science/article/pii/S0925838801008817*

Halevy I, Zenou V Y, Salhov S, Caspi E N, Schäfer W & Yaar I 2006 Journal of Alloys and Compounds **419**(1), 21–24.
URL: *https://www.sciencedirect.com/science/article/pii/S0925838805015161*

Hill H H 1970 Plutonium 1970 and Other Actinides: Proceedings number ptie. 1 in 'Nuclear metallurgy' Metallurgical Society of the American Institute of Mining, Metallurgical, and Petroleum Engineers.
URL: *https://books.google.pl/books?id=QK7jSQAACAAJ*

Hirschberger M, Nakajima T, Gao S, Peng L C, Kikkawa A, Kurumaji T, Kriener M, Yamasaki Y, Sagayama H, H. N, K. O, Kakurai K, Taguchi Y, Yu X, Arima T & Tokura Y 2019 Nature Commun. **10**, 5831.
URL: *https://www.nature.com/articles/s41467-019-13675-4*

Huang K, Nelson W L, Chemey A T, Albrecht-Schmitt T E & Baumbach R E 2019 J. Phys.:Cond. Matter **31**, 165601.
URL: *https://iopscience.iop.org/article/10.1088/1361-648X/aafe9e*

Kangas M J, Treadwell L J, Haldolaarachchige N, McAlpin J D, Young D P & Chan J Y 2013 J. Solid State Chem. **197**, 523–531.
URL: *https://www.sciencedirect.com/science/article/pii/S0022459612005257*

Kase N, Satoh R, Nakano T & Takeda N 2016 J. Phys. Soc. Jpn. **85**, 105001.
URL: *https://journals.jps.jp/doi/10.7566/JPSJ.85.105001*

Leenaers A, Wight J, Van den Berghe S, Ryu H J & Valery J-F 2020a Vol. 5 Elsevier pp. 499–530.
URL: *https://www.sciencedirect.com/science/article/pii/B9780128035818117758*

Leenaers A, Wight J, Van den Berghe S, Ryu H J & Valery J-F 2020b Vol. 5 Elsevier pp. 485–498.
URL: *https://www.sciencedirect.com/science/article/pii/B9780128035818116078*

Lhotel E, Jaubert L D C & Holdsworth P C W 2020 J. Low. Temp. Phys. **201**, 710–737.
URL: *https://link.springer.com/article/10.1007/s10909-020-02521-3*

Liu P, Xian Y, Wang X, Zhang Y & Zhang P 2017 J. Nucl. Mater. **493**, 147–153.
URL: *https://www.sciencedirect.com/science/article/pii/S0022311516313125*

Matsumoto Y, Matsuda T D, Tateiwa N, Yamamoto E, Haga Y & Fisk Z 2013 J. Korean Phys. Soc. **63**, 363–366.
URL: *https://link.springer.com/article/10.3938/jkps.63.363*

Maurya A, Thamizhavel A & Dhar S K 2014 AIP Conf. Proc. **1591**, 1642–1644.
URL: *https://aip.scitation.org/doi/abs/10.1063/1.4873062*

Meisner G P 1981 Physica B&C **108**, 763–764.
URL: *https://www.sciencedirect.com/science/article/pii/0378436381906860*

Meshi L, Zenou V Y, Ezersky V, Munitz A & Talianker M 2002 Journal of Alloys and Compounds **347**(1), 178–183.
URL: *https://www.sciencedirect.com/science/article/pii/S0925838802007740*

Moussa C, Berche A, Pasturel M, Barbosa J, Stepnik B, Dubois S & Tougait O 2017 J. Alloys Compd. **691**, 893–905.
URL: *https://www.sciencedirect.com/science/article/pii/S0925838816326573*

Moussa C, Désévédavy F, Noël H, Pasturel M, Gouttefangeas F, Dubois S, Stepnik B & Tougait O

2015 J. Nucl. Mater. **461**, 193–199.
URL: *https://www.sciencedirect.com/science/article/pii/S0022311515001531*
Moussa C, Pasturel M, Stepnik B & Tougait O 2015 Intermetallics **57**, 1–6.
URL: *https://www.sciencedirect.com/science/article/pii/S0966979514002581*
Nakamura S, Kabeya N, Kobayashi M, Araki K, Katoh K & Ochiai A 2018 Phys. Rev. B **98**, 054410.
URL: *https://journals.aps.org/prb/abstract/10.1103/PhysRevB.98.054410*
Nazaré S, Ondracek G & Thümmler F 1975 J. Nucl. Mater. **56**, 251–259.
URL: *https://www.sciencedirect.com/science/article/pii/0022311575900409*
Niemann S & Jeitschko W 1995a J. Solid State Chem. **116**, 131–135.
URL: *https://www.sciencedirect.com/science/article/pii/S0022459685711930*
Niemann S & Jeitschko W 1995b J. Solid State Chem. **114**, 337–341.
URL: *https://www.sciencedirect.comr/science/article/pii/S0022459685710523*
Noël H, Gonçalves A & Waerenborgh J 2004 Intermetallics **12**(2), 189–194.
URL: *https://www.sciencedirect.com/science/article/pii/S0966979503002164*
Noël H, Tougait O & Dubois S 2009 J. Nucl. Mater **389**, 93–97.
URL: *https://www.sciencedirect.com/science/article/pii/S0022311509000221*
Noël H, Tougait O, Troć R & Zaremba V 2005 Solid State Sci. **7**, 780–783.
URL: *https://www.sciencedirect.com/science/article/pii/S1293255805000828*
Ogunbunmi M O, Nair H S & Strydom A M 2022 Crit. Rev. Solid State Mater. Sci. .
URL: *https://www.tandfonline.com/doi/abs/10.1080/10408436.2022.2075827?journalCode=bsms20*
Okuda K, Noguchi S, Nakazawa Y & Ishikawa M 1989 J. Phys. Soc. Jpn **58**, 4296–4299.
URL: *https://journals.jps.jp/doi/10.1143/JPSJ.58.4296*
Pasturel M, Tougait O, Potel M, Roisnel T, Wochowski K, Noël H & Troć R 2009 J. Phys.: Cond. Mat. **21**, 125401.
URL: *https://iopscience-iop-org.inc.bib.cnrs.fr/article/10.1088/0953-8984/21/12/125401*
Prokeš K, Bartkowiac M, Gorbunov D I, Prokhnenko O, Rivin O & Smeibidl P 2020 Phys. Rev. Res. **2**, 013137.
URL: *https://journals.aps.org/prresearch/abstract/10.1103/PhysRevResearch.2.013137*
Rabin D, Schneck R Z, Rafailov G, Dahan I, Meshi L & Brosh E 2015 J. Nucl. Mater. **464**, 170–184.
URL: *https://www.sciencedirect.com/science/article/pii/S0022311515002305*
Raposio R, Thorogood G, Czerwinski K & Rozenfeld A 2019 Appl. Radiat. Isotopes **148**, 225–231.
URL: *https://www.sciencedirect.com/science/article/pii/S0969804318309436*
Reig-i-Plessis D & Hallas A M 2021 Phys. Rev. Mater. **5**, 030301.
URL: *https://journals.aps.org/prmaterials/abstract/10.1103/PhysRevMaterials.5.030301*
Ryu H J, Kim C K, Sim M, Park J M & Lee J H 2013 Nucl. Eng. Technol. **45**, 979–986.
URL: *https://www.sciencedirect.com/science/article/pii/S1738573315300838*
Samsel-Czekała M, Talik E, Pasturel M & Troć R 2013 Journal of Alloys and Compounds **554**, 438–445.
URL: *https://www.sciencedirect.com/science/article/pii/S0925838812021950*
Shastry B S & Sutherland B 1981 Phys. Rev. Lett. **47**, 964–967.
URL: *https://journals.aps.org/prl/abstract/10.1103/PhysRevLett.47.964*
Shtrikman S & Wohlfarth E P 1981 Phys. Lett. A **85**, 467–470.
URL: *https://www.sciencedirect.com/science/article/pii/0375960181904412*
Snelgrove J L, Hofman G L, Meyer M K, Trybus C L & Wiencek T C 1997 Nucl. Eng. Design **178**, 119–126.
URL: *https://www.sciencedirect.com/science/article/pii/S0029549397002173*
Sugai T, Haga Y, Matsuda T D, Yamamoto E, Tateiwa N, Honda F, Settai R & Onuki Y 2011 Journal of Physics: Conference Series **273**, 012122.
URL: *https://iopscience.iop.org/article/10.1088/1742-6596/273/1/012122*
Süllow S, Nieuwenhuys G J, Menovsky A A, Mydosh J A, Mentnik S A M, Mason T E & Buyers W J L 1997 Phys. Rev. Lett. **78**, 354–357.
URL: *https://journals.aps.org/prl/abstract/10.1103/PhysRevLett.78.354*

Swain N, Shahzad M & Sengupta P 2022 arXiv:2203.03359v1 .
URL: *https://arxiv.org/abs/2203.03359*
Swatek P & Kaczorowski D 2012 Journal of Solid State Chemistry **191**, 191–194.
URL: *https://www.sciencedirect.com/science/article/pii/S0022459612001831*
Swatek P, Kleinert M, Wiśniewski P & Kaczorowski D 2018 Computational Materials Science **153**, 461–472.
URL: *https://www.sciencedirect.com/science/article/pii/S0927025618304269*
Thalmeier P 2002 Eur. Phys. J B **27**, 29–48.
URL: *https://link.springer.com/article/10.1140/epjb/e20020127*
Tokura Y, Yasuda K & Tsukazaki A 2019 Nature Rev. Phys. **1**, 126–143.
URL: *https://www.nature.com/articles/s42254-018-0011-5*
Tougait O, Noël H & Troć R 2004 J. Solid State Chem. **177**, 2053–2057.
URL: *https://www.sciencedirect.com/science/article/pii/S0022459604000696*
Tougait O, Stępień-Damm J, Zaremba V, Noël H & Troć R 2003 J. Solid State Chem. **174**, 152–158.
URL: *https://www.sciencedirect.com/science/article/pii/S0022459603001919*
Tougait O, Troć R, Zaleski A & Noël H 2007 Phil. Mag. **87**, 1085–1095.
URL: *https://www.tandfonline.com/doi/full/10.1080/14786430601026479*
Treadwell L J, Watkins-Curry P, McAlpin J D, Prestigiacomo J, Stadler S & Chan J Y 2014 J. Solid State Chem. **210**, 267–274.
URL: *https://www.sciencedirect.com/science/article/pii/S0022459613005677*
Troć R, Bukowski Z, Sulkowski C, Morkowski J A, Szajek A & Chelkowska G 2005 Physica B-Cond. Matter **359**, 1375–1377.
URL: *https://www.sciencedirect.com/science/article/pii/S0921452605004564*
Troć R, Gajek Z, Pasturel M, Wawryk R & Samsel-Czekała M 2019 Intermetallics **107**, 60–74.
URL: *https://www.sciencedirect.com/science/article/pii/S0966979518307611*
Troć R, Noël H, Tougait O & Wochowski K 2004 J. Phys.:Cond. Matter **16**, 3097–3106.
URL: *https://iopscience.iop.org/article/10.1088/0953-8984/16/18/011*
Troć R, Pasturel M, Samsel-Czekała M, Wawryk R & Gajek Z 2018 Journal of Alloys and Compounds **742**, 656–669.
URL: *https://www.sciencedirect.com/science/article/pii/S0925838818303335*
Troć R, Pasturel M, Tougait O, Sazonov A P, Gukasov A, Sulkowski C & Noël H 2012 Phys. Rev. B **85**, 064412.
URL: *https://journals.aps.org/prb/abstract/10.1103/PhysRevB.85.064412*
Troć R, Samsel-Czekała M, Talik E, Wawryk R, Gajek Z & Pasturel M 2015 Phys. Rev. B **92**, 104427.
URL: *https://link.aps.org/doi/10.1103/PhysRevB.92.104427*
Troć R, Tran V H, Vagizov F G & Drulis H 1993 J. Alloys Compd. **200**, 37–42.
URL: *https://www.sciencedirect.com/science/article/pii/0925838893904683*
Troć R, Wawryk R, Gajek Z, Pasturel M & Samsel-Czekała M 2017 Journal of Alloys and Compounds **727**, 1302–1313.
URL: *https://www.sciencedirect.com/science/article/pii/S0925838817329559*
Troć R, Pasturel M, Tougait O, Potel M & Noël H 2011 Intermetallics **19**(7), 913–918.
URL: *https://www.sciencedirect.com/science/article/pii/S0966979511000392*
Turner J, Martini F, Buckley J, Phillips G, Middleburgh S C & Abram T J 2020 J. Nucl. Mater. **540**, 152388.
URL: *https://www.sciencedirect.com/science/article/pii/S002231152030996X*
Verbovytsky Yu & Gonçalves A P 2013 Intermetallics **33**, 16–26.
URL: *https://www.sciencedirect.com/science/article/pii/S0966979512003779*
Verbovytsky Yu, Łątka K & Tomala K 2008 J. Alloys Compd. **450**, 114–117.
URL: *https://www.sciencedirect.com/science/article/pii/S092583880700607X*
Wallenius J 2020 Vol. 5 Elsevier pp. 88–101.
URL: *ttps://www.sciencedirect.com/science/article/pii/B9780128035818116947*

Wang C H, Lawrence J M, Bauer E D, Kothapalli K, Gardner J S, Ronning F, Gofryk K, Thompson J D, Nakotte H & Trouw F 2010 Phys. Rev. B **82**, 094406.
URL: *https://journals.aps.org/prb/abstract/10.1103/PhysRevB.82.094406*

Weitzer F, Potel M, Noël H & Rogl P 1994 J. Solid State Chem. **111**, 267–275.
URL: *https://www.sciencedirect.com/science/article/pii/S0022459684712278*

Winiarski M J, Griveau J C, Colineau E, Wochowski K, Wiśniewski P, Kaczorowski D, Caciuffo R & Klimczuk T 2017 Journal of Alloys and Compounds **696**, 1113–1119.
URL: *https://www.sciencedirect.com/science/article/pii/S092583881633941X*

Wiśniewski P, Swatek P, Gukasov A & Kaczorowski D 2012 Phys. Rev. B **86**, 054438.
URL: *https://link.aps.org/doi/10.1103/PhysRevB.86.054438*

Wolff M W, Niemann S, Ebel T & Jeitschko W 2001 J. Magn. Magn. Mater. **223**, 1–15.
URL: *https://www.sciencedirect.com/science/article/pii/S0304885300005369*

Yağcı N K 2021 Philosophical Magazine **101**(8), 1019–1032.
URL: *https://doi.org/10.1080/14786435.2021.1876266*

Zenou V Y, Meshi L & Fuks D 2011 Intermetallics **19**(5), 713–720.
URL: *https://www.sciencedirect.com/science/article/pii/S0966979511000306*

Zwicknagl G, Yaresko A N & Fulde P 2002 Phys. Rev. B **65**, 081103.
URL: *https://link.aps.org/doi/10.1103/PhysRevB.65.081103*